

Vortex disruption by magnetohydrodynamic feedback

J. Mak,* S. D. Griffiths, and D. W. Hughes

Department of Applied Mathematics, University of Leeds, Leeds, LS2 9JT, UK

In an electrically conducting fluid, vortices stretch out a weak, large-scale magnetic field to form strong current sheets on their edges. Associated with these current sheets are magnetic stresses, which are subsequently released through reconnection, leading to vortex disruption, and possibly even destruction. This disruption phenomenon is investigated here in the context of two-dimensional, homogeneous, incompressible magnetohydrodynamics. We derive a simple order of magnitude estimate for the magnetic stresses — and thus the degree of disruption — that depends on the strength of the background magnetic field (measured by the parameter M , a ratio between the Alfvén speed and a typical flow speed) and on the magnetic diffusivity (measured by the magnetic Reynolds number R_m). The resulting estimate suggests that significant disruption occurs when $M^2 R_m = O(1)$. To test our prediction, we analyse direct numerical simulations of vortices generated by the breakup of unstable shear flows with an initially weak background magnetic field. Using the Okubo–Weiss vortex coherence criterion, we introduce a vortex disruption measure, and show that it is consistent with our predicted scaling, for vortices generated by instabilities of both a shear layer and a jet.

* julian.c.l.mak@googlemail.com; Current address: Department of Physics, University of Oxford, Clarendon Laboratory, Parks Road Oxford, OX1 3PU

I. INTRODUCTION

The interaction of vortices with a magnetic field is a fundamental process in astrophysical magnetohydrodynamics (MHD). Such vortices could be generated, for example, by convection [1, 2] or by the breakup of unstable shear flows [3–6]. In the absence of magnetic fields, vortices can be coherent, long-lived structures, particularly in two-dimensional or quasi-two-dimensional systems [e.g., 7]. However, in the presence of a background magnetic field, various studies have shown how vortices can be disrupted, by which we mean either a reduction in strength or spatial coherence, or completely destroyed [8–16]. Here we show explicitly how this disruption depends on both the field strength and on the magnetic Reynolds number Rm .

Astrophysical fluid flows are invariably characterised by extremely high values of Rm . Perhaps the most important consequence of this is that weak large-scale fields can be stretched by the flow to generate strong small-scale fields, with the amplification being some positive power of Rm [17]. Once the small-scale fields are dynamically significant, the resulting evolution is essentially magnetohydrodynamic — rather than hydrodynamic — leading to dramatically different characteristics, despite the large-scale magnetic field being very weak. Such behaviour has been identified in the suppression of turbulent transport [18–24], in the suppression of jets in β -plane turbulence [25], and in the inhibition of large-scale vortex formation in rapidly rotating convection [26].

The vortex disruption investigated here, which builds on [27], and can be contrasted with [28], depends on just such high Rm dynamics. Given that many astrophysical flows are rotating and stratified, such that the vortices are essentially two-dimensional, it is natural to investigate vortex disruption in the context of two-dimensional MHD. In order to quantify when a weak large-scale field can become dynamically significant, we first construct a scaling argument for a quite general setting with a single vortex. We first estimate the amplification of the large-scale field due to stretching on the edge of the vortex, following the kinematic arguments of Weiss [29], and then estimate the dynamical feedback on the vorticity. This leads to an explicit prediction for vortex disruption in terms of the strength of the large-scale field and Rm .

To investigate vortex disruption in more realistic settings it is necessary to perform direct numerical simulations of the governing MHD equations for freely evolving flows. The vortices may be imposed via the initial conditions or, alternatively, may emerge from the development of an instability of a basic state. Here we adopt the latter approach by considering the instability to two-dimensional perturbations of two representative incompressible planar shear flows — a shear layer and a jet — with an aligned magnetic field. This typically leads to the generation of a periodic array of vortices, each of which may be susceptible to disruption by the magnetic field. Any other potential disruption mechanism that requires stratification (e.g., convective instability in the vortex core due to overturning density surfaces [4, 5]) or a third spatial dimension (e.g., elliptic instability [30, 31] or the magnetoelliptic instability [32, 33]) is ruled out in our numerical simulations, thereby isolating the magnetic field as the sole agent of vortex disruption.

Since magnetic dissipation is crucial in determining the eventual strength of the small-scale fields, and hence the efficacy of the vortex disruption mechanism, it is important to consider how this is implemented numerically. In order to have well-defined values of Rm , we carry out simulations with explicit Ohmic dissipation, represented by a Laplacian, with resolution to the dissipative scale. This is in contrast to most other studies of vortex disruption in MHD, in which dissipation is performed numerically at the grid scale, with no explicit diffusion operator [8–10, 12–15].

The plan of the article is as follows. Section II contains the scaling argument for the disruption of a single vortex. The mathematical and numerical formulation of the shear flow problem is given in Section III. Section IV contains the numerical simulations of vortex disruption; a measure of disruption based on the Okubo–Weiss criterion [34, 35] is introduced and is used to test the main prediction of Section II. Armed with the results of the numerical simulations, in Section V we examine in detail the scaling arguments outlined in Section II. In Section VI we look at the implications for the large-scale dynamics of the shear flow instability, with particular focus on the mean flow. We conclude in Section VII, and briefly discuss possible implications of vortex disruption for the transition to turbulence and mixing.

II. THEORETICAL ESTIMATE OF VORTEX DISRUPTION

Following Weiss [29], we consider an idealised configuration in which a single vortex evolves kinematically in an initially uniform magnetic field of strength B_0 . On an advective timescale, the fluid motion stretches the weak background field on the edges of the vortex until reconnection of field lines occurs; subsequently, the magnetic field lines within the vortex reconnect and are expelled to the edges of the vortex, a phenomenon known as flux expulsion. Weiss was particularly interested in determining the scalings of the flux-expelled state, as were Moffatt & Kamkar [36]. Here, however, we are interested in the peak field at the point of reconnection at the edges of the vortex (Weiss’s B_1). Since the curved field lines have associated with them magnetic stresses directed towards the vortex centre, then if B_1 is sufficiently strong, the induced stresses will be significant, and we might expect vortex disruption. We are then able to provide an estimate for the dependence of disruption on B_0 and the magnetic diffusivity η , using an essentially kinematic argument; put another way, the theory here estimates when the kinematic approach breaks down and there must be significant dynamical feedback. This approach is similar in spirit to that of Galloway and co-workers [37, 38], who considered the dynamical feedback of flux ropes formed in magnetoconvection. More recently, Gilbert *et*

al. [28] also considered the dynamical feedback on a vortex, in an idealised, quasi-linear setting in which only the axisymmetric component of the Lorentz force was retained, thus constraining the vortex flow to remain axisymmetric; this distinguishes it from the fully nonlinear problem considered here.

The magnetic field is governed by the induction equation

$$\frac{\partial \mathbf{B}}{\partial t} = \nabla \times (\mathbf{u} \times \mathbf{B}) + \eta \nabla^2 \mathbf{B}. \quad (1)$$

We suppose that the vortex has characteristic length L_v and velocity U_v . The initial large-scale field B_0 is amplified to a stronger small-scale field of strength b and with a small characteristic scale ℓ . Flux conservation across the vortex implies that

$$b\ell = B_0 L_v. \quad (2)$$

Following the physical arguments of Weiss [29], field amplification is arrested when line stretching and magnetic diffusion are in balance, i.e. when $|\mathbf{B} \cdot \nabla \mathbf{u}| \sim \eta |\nabla^2 \mathbf{B}|$, or $U_v B_0 / L_v \sim \eta b / \ell^2$. Combining this expression with (2) gives

$$b \sim \left(\frac{U_v L_v}{\eta} \right)^{1/3} B_0. \quad (3)$$

The same estimate was obtained via alternative means in [36].

At this stage of the evolution, the magnetic stresses resulting from the Lorentz force may be estimated. We are interested in the magnetic tension, which may be decomposed as

$$\frac{1}{\mu_0} \mathbf{B} \cdot \nabla \mathbf{B} = -\frac{|\mathbf{B}|^2}{\mu_0 r_c} \mathbf{e}_n + \frac{d}{ds} \left(\frac{|\mathbf{B}|^2}{2\mu_0} \right) \mathbf{e}_t, \quad (4)$$

where μ_0 is the permeability of free space, r_c is the local radius of curvature, s is the arc length, and \mathbf{e}_n and \mathbf{e}_t are, respectively, the local unit vectors normal and tangential to the magnetic field. For a field expelled to the edge of the vortex, $|\mathbf{B}| \sim b$, $r_c \sim L_v$, and $d/ds \sim L_v^{-1}$; hence

$$\frac{1}{\mu_0} |\mathbf{B} \cdot \nabla \mathbf{B}| \sim \frac{b^2}{\mu_0 L_v}. \quad (5)$$

To estimate when the magnetic tension will be dynamically important in the evolution of the vortex, we consider the vorticity equation

$$\frac{\partial \boldsymbol{\omega}}{\partial t} + \mathbf{u} \cdot \nabla \boldsymbol{\omega} - \boldsymbol{\omega} \cdot \nabla \mathbf{u} = \frac{1}{\mu_0 \rho} \nabla \times (\mathbf{B} \cdot \nabla \mathbf{B}) + \nu \nabla^2 \boldsymbol{\omega}, \quad (6)$$

where ρ is the constant density of the fluid. The curl of the magnetic tension involves a transverse derivative of the tangential component, and using (5), thus scales as $b^2 / (\mu_0 \ell L_v)$. We may characterise the vortex disruption regime as one in which the curl of the magnetic tension competes with the advection of vorticity, thereby leading to the scaling

$$\frac{1}{\mu_0 \rho} \frac{b^2}{\ell L_v} \sim \frac{U_v}{L_v} \tilde{\Omega}_v, \quad (7)$$

where $\tilde{\Omega}_v \sim U_v / L_v$ is the vorticity. Note that here we are assuming that disruption of the vortex, if it occurs, does so on a much faster timescale than that for reaching the flux-expelled state. Using expressions (2) and (3), the estimate (7) may be written as

$$\frac{B_0^2 / (\mu_0 \rho)}{\eta} \sim \tilde{\Omega}_v. \quad (8)$$

Expression (8) is the dimensional estimate for vortex disruption in terms of the characteristic scales of the vortex. Typically, however, there are other velocity and length scales, U_0 and L_0 , that are used to characterise the flow. Retaining B_0 as the characteristic field strength, the relevant non-dimensional parameters are

$$M = \frac{B_0 / \sqrt{\mu_0 \rho}}{U_0}, \quad \text{Rm} = \frac{U_0 L_0}{\eta}, \quad (9)$$

where M , the ratio of the Alfvén speed to the characteristic flow speed, is a measure of field strength. Expression (8) may thus be written as

$$M^2 \text{Rm} \sim \Omega_v, \quad (10)$$

where

$$\Omega_v = \frac{U_v/L_v}{U_0/L_0} \quad (11)$$

is the non-dimensional magnitude of the vortex. In many settings, L_v and U_v will be comparable with L_0 and U_0 , in which case the non-dimensional estimate for vortex disruption becomes

$$M^2 \text{Rm} \sim 1. \quad (12)$$

The scaling provided by (12), first given in [27], will be tested against simulation data presented in Section IV. The arguments concerning length scales, leading to the estimate (8), will be revisited in detail in Section V.

III. MATHEMATICAL AND NUMERICAL FORMULATION

To examine vortex disruption in detail, we consider the evolution of unstable shear flows of the form $\mathbf{u} = U(y)\mathbf{e}_x$, in the presence of a uniform background magnetic field $\mathbf{B} = B_0\mathbf{e}_x$, in two-dimensional incompressible MHD. Since both \mathbf{u} and \mathbf{B} are divergence-free, they may be expressed in terms of a streamfunction and magnetic potential, defined by

$$\mathbf{u} = (u, v, 0) = \nabla \times (\psi \mathbf{e}_z), \quad \mathbf{B} = \nabla \times (A \mathbf{e}_z). \quad (13)$$

The z -components of the vorticity and current are then given by $\omega = -\nabla^2 \psi$ and $\mu_0 j = -\nabla^2 A$ respectively. On scaling velocity with a representative flow speed U_0 , length with a characteristic scale L_0 , time with L_0/U_0 , and magnetic field with B_0 , the non-dimensional governing equations become

$$\frac{\partial \omega}{\partial t} - J(\psi, \omega) - M^2 J(A, \nabla^2 A) = \frac{1}{\text{Re}} \nabla^2 \omega, \quad (14a)$$

$$\frac{\partial A}{\partial t} - J(\psi, A) = \frac{1}{\text{Rm}} \nabla^2 A, \quad (14b)$$

$$-\nabla^2 \psi = \omega, \quad (14c)$$

where

$$J(f, g) = \frac{\partial f}{\partial x} \frac{\partial g}{\partial y} - \frac{\partial f}{\partial y} \frac{\partial g}{\partial x} \quad (15)$$

is the Jacobian operator. The non-dimensional parameters are M and Rm , as defined in (9), and the Reynolds number

$$\text{Re} = \frac{U_0 L_0}{\nu}, \quad (16)$$

where ν is the kinematic viscosity. In non-dimensional form, the two flow profiles we shall consider are $U(y) = \tanh(y)$ and $U(y) = \text{sech}^2(y)$, which we shall refer to as the shear layer and the jet respectively.

We further decompose the variables in terms of a basic state and a perturbation, i.e.,

$$\psi = \Psi(y) + \tilde{\psi}, \quad A = y + \tilde{A}, \quad \omega = -U'(y) + \tilde{\omega}, \quad (17)$$

where a prime denotes differentiation with respect to y . The system of equations (14) then takes the equivalent formulation (after dropping the tildes on the perturbation terms)

$$\frac{\partial \omega}{\partial t} + U \frac{\partial \omega}{\partial x} - U'' \frac{\partial \psi}{\partial x} - J(\psi, \omega) - M^2 \left[-\frac{\partial \nabla^2 A}{\partial x} + J(A, \nabla^2 A) \right] = \frac{1}{\text{Re}} \nabla^2 \omega - \frac{1}{\text{Re}} U''', \quad (18a)$$

$$\frac{\partial A}{\partial t} + U \frac{\partial A}{\partial x} - \frac{\partial \psi}{\partial x} - J(\psi, A) = \frac{1}{\text{Rm}} \nabla^2 A, \quad (18b)$$

$$-\nabla^2 \psi = \omega. \quad (18c)$$

We adopt a domain that is periodic in x and bounded by impermeable, perfectly conducting and stress-free walls at $y = \pm L_y$, leading to the boundary conditions

$$\psi = 0, \quad A = 0, \quad \omega = 0 \quad \text{on} \quad y = \pm L_y. \quad (19)$$

The total energy (the sum of the kinetic energy E_k and the magnetic energy E_m) decays as

$$\frac{d}{dt}(E_k + E_m) = -\frac{1}{\text{Re}} \iint \omega^2 dx dy - \frac{1}{\text{Rm}} \iint j^2 dx dy, \quad (20)$$

where E_k and E_m are the domain integrals of $|\mathbf{u}|^2/2$ and $M^2|\mathbf{B}|^2/2$, respectively.

The channel length is chosen to be some integer multiple of the most unstable wavelength from linear theory, i.e., $L_x = 2n\pi/\alpha_c$, where α_c is the most unstable wavenumber of the associated profiles ($\alpha_c = 0.44$ for the shear layer and $\alpha_c = 0.90$ for the jet [39]). We take $n = 1$ for the shear layer and $n = 2$ for the jet, giving domains of roughly equal size. To trigger the instability, we initialise with a perturbation for which the primary instability at wavenumber α_c has fixed amplitude and phase, with other permitted wavenumbers α_i having smaller amplitude and random phase. Specifically, we take

$$(\omega, A) = \left[10^{-3} \cos(\alpha_c x) + 10^{-5} \sum_{i \neq n}^{\lfloor N_x/3 \rfloor} \gamma_i \cos(\alpha_i x - \sigma_i L_x) \right] e^{-y^2}, \quad (21)$$

where γ_i and σ_i are randomly generated numbers in $[-1, 1]$, and $\lfloor \cdot \rfloor$ is the floor function. There is a well-defined linear phase of instability, during which the most unstable eigenfunction naturally emerges. Simulations were run up to $t = 150$, allowing for an extended nonlinear phase and the possibility of vortex disruption; with this choice we find that taking $L_y = 10$ ensures that finite boundary effects remain negligible.

We solve the system of equations (18) by a Fourier–Chebyshev pseudo-spectral method, using the standard Fourier collocation points in x and Gauss–Lobatto points in y , and employing the appropriate Fast Fourier Transforms. A semi-implicit treatment in time is employed, treating the dissipation terms implicitly and the nonlinear terms explicitly. Time-stepping is performed by a third-order accurate, variable time-step, Adams–Bashforth/Backward-Difference scheme, with the step size set by the maximum time step allowed for a fixed CFL number (here taken to be 0.2, which is near marginal for numerical stability). The equations are solved in spectral space using a fast Helmholtz solver [40], and all runs are dealiased using Orszag’s 2/3-rule [41] (see [42] or [43] for further details about the numerical methods employed).

Our simulations are run-down experiments for the evolution of instabilities on a decaying background state. To alleviate diffusive effects before the perturbations reach finite amplitude, we remove the diffusion of the basic state (the U''' term in (18a)) until the perturbation is sufficiently large (here measured by the energy possessed by the $k_x \neq 0$ Fourier modes). Even so, we found it necessary to take $\text{Re} \gtrsim 500$ in order to produce runs that are not too diffusive and that are qualitatively similar to the runs at higher Re . Since the regime estimate (12) naturally suggests a dependence on M and Rm , we fix $\text{Re} = 500$ and vary the other two parameters in the bulk of this work. The required spatial resolution depends on Rm : the number of x -gridpoints N_x and y -gridpoints N_y were taken to be $N_x \times N_y = 512 \times 1024$ for $\text{Rm} = 1000$, 384×768 for $\text{Rm} = 750$, and 256×512 otherwise.

IV. VORTEX DISRUPTION

In this section, we describe the results of direct numerical simulations of freely evolving vortices generated by shear instabilities with a background magnetic field. To measure the disruption of the vortices, we follow Okubo [34] and Weiss [35] in considering the quantity $W(x, y, t)$, defined by

$$W = \left(\frac{\partial u}{\partial x} - \frac{\partial v}{\partial y} \right)^2 + \left(\frac{\partial v}{\partial x} + \frac{\partial u}{\partial y} \right)^2 - \left(\frac{\partial v}{\partial x} - \frac{\partial u}{\partial y} \right)^2. \quad (22)$$

The bracketed terms are respectively the normal and shear components of the rate of strain, and the vorticity; W thus effectively measures the relative dominance of the strain over the vorticity. A vortex is defined as a region in which W is sufficiently negative. For example, a popular approach is to calculate the standard deviation σ of W and to classify vortical regions by $W < -0.2\sigma$. Though by no means the only way to identify a vortex [e.g., 44–46], it is one of the simpler measures that have been employed previously in a geophysical setting [e.g., 47, 48].

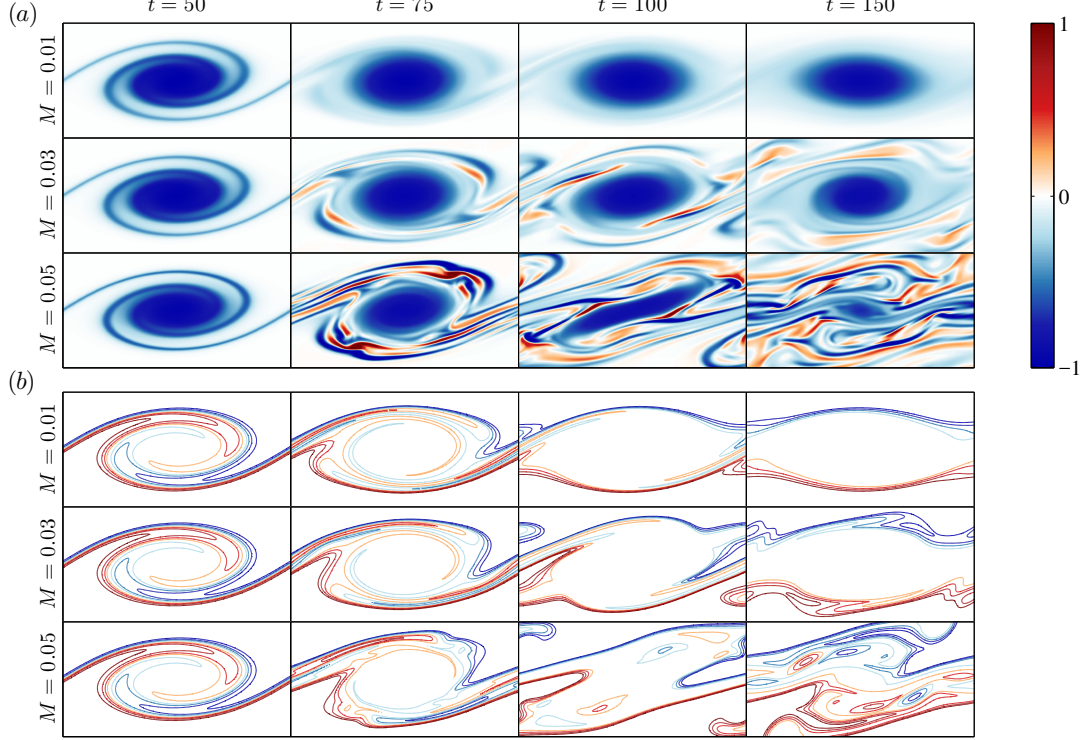
Here we are interested in measuring vortex disruption relative to the purely hydrodynamic evolution. We thus introduce a vortex disruption parameter $\Delta(t)$, defined by

$$\Delta = 1 - \frac{\int_A W dx dy}{\int_A W_{\text{HD}} dx dy}, \quad (23)$$

where W_{HD} is the value of W for the hydrodynamic case. The area A is some portion of physical space where there is deemed to be a vortex, as discussed in more detail below. When $\Delta = 0$, the vortex is not disrupted, whereas $\Delta = 1$ implies total disruption.

parameter	values	marker/colour in Fig. 4
M	0.01–0.1, 0.01 spacing	+ ○ * × □ ◇ △ ▽ ☆ ✕, in ascending order
Rm	50, 250, 500, 750, 1000	black, red, green, blue, magenta

TABLE I. Parameter values employed for the shear layer simulations.

FIG. 1. Snapshots of (a) vorticity and (b) magnetic field lines for the shear layer at different field strengths (for $Rm = Re = 500$), shown for the central half of the channel ($-L_y/2 \leq y \leq L_y/2$).

A. Hyperbolic-tangent shear layer

We first consider the disruption of vortices arising from the instability of the shear layer $U(y) = \tanh(y)$. Linear instabilities of this profile are well documented for both the hydrodynamic [39] and MHD cases, where linear stability is guaranteed when $M \geq 1$ [49, 50]. The nonlinear MHD evolution has been studied by numerous authors [e.g., 8–10, 12, 14, 16]. In order to provide a good coverage of (M, Rm) space, a total of fifty simulations with parameter values given in Table I were performed, at five values of Rm and ten values of M , where the values of M were chosen to lie well below the stabilising value of M ($M \approx 0.8$ for $\alpha = 0.44$). The initial magnetic to kinetic energy ratio is given by $2M^2 L_y / (\int U(y)^2 dy) \approx (10/9)M^2$; this ratio is less than $1/90$ for the values of M considered here.

We consider a domain supporting a single wavelength of the optimum linear instability mode. Fig. 1 shows snapshots of the vorticity and magnetic field lines from three control runs at $Rm = 500$. These display the representative behaviours for three dynamical regimes: undisturbed ($M = 0.01$), mildly disrupted ($M = 0.03$) and severely disrupted ($M = 0.05$). For $M = 0.01$, the vorticity is of one sign, and the shear layer rolls up into a vortex. The magnetic stresses are clearly not strong enough to alter the macro-dynamics in any significant way. The vortex evolution is essentially hydrodynamic [7], accompanied by magnetic flux expulsion from the vortex. For $M = 0.03$, we observe the formation of regions of positive vorticity. The magnetic field is no longer confined to kinematic boundary layers, and the resulting stresses are strong enough to modify the resulting evolution to a certain extent. That said, the vortex is only mildly disrupted and maintains its integrity; there is only a slight decrease of vortex size by the end of the simulation at $t = 150$. For $M = 0.05$, the evolution is radically different to the other two cases, with a significant disruption of the vortex and an unconfined magnetic field. By the end of the simulation, only small remnants of the parent vortex persist; vorticity filaments and a complex magnetic field are now the dominant features in the domain.

Vortex disruption also has a signature in the time evolution of the kinetic and magnetic energies. Shown in Fig. 2 are time

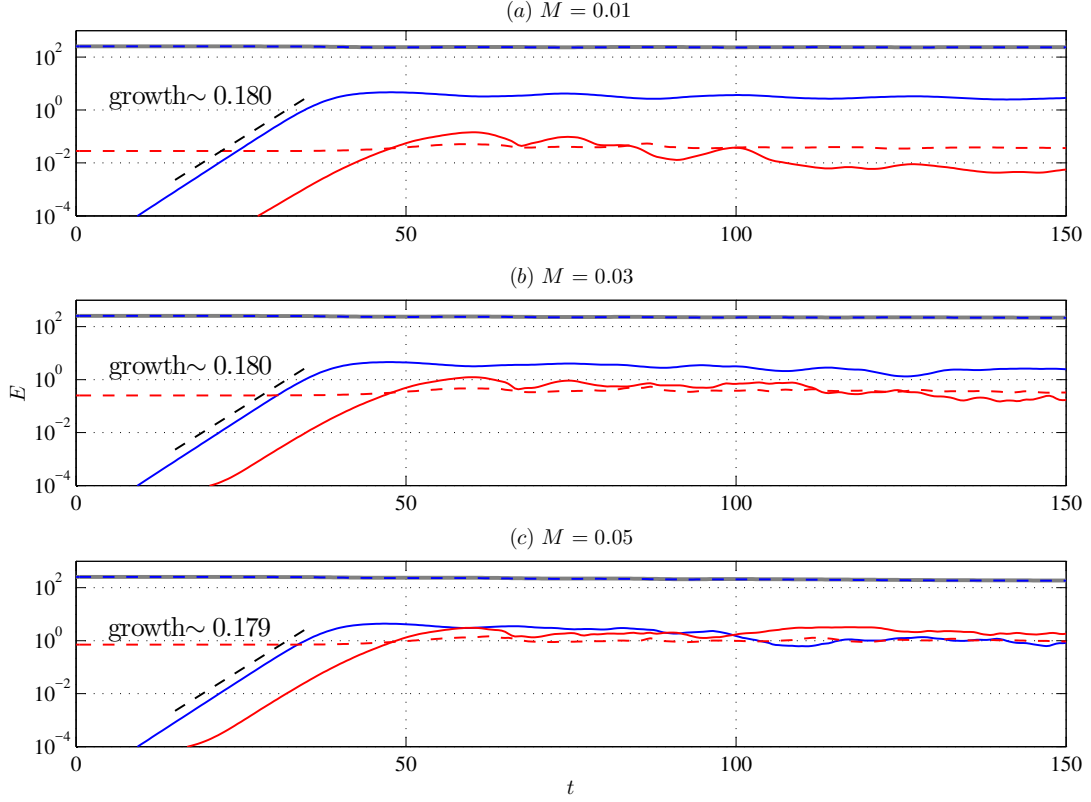


FIG. 2. Time series of the energies (blue = kinetic; red = magnetic; solid = perturbation state; dashed = mean state; grey solid line = total energy) for the shear layer at different field strengths (for $\text{Rm} = \text{Re} = 500$). The curve for mean kinetic energy largely lies on top of the curve for the total energy.

series for the three control runs of the mean kinetic energy \bar{E}_k and mean magnetic energy \bar{E}_m (defined as the energy content in the $k_x = 0$ Fourier mode), along with the perturbation energies E'_k and E'_m (defined as the energy content in the remaining Fourier modes). The evolution is similar up to $t \approx 60$ (cf. Fig. 1), at which time the field amplification is close to being arrested by diffusion; the scalings (2) and (3) then apply for the small-scale field, implying $E'_m \sim b^2 l L_v$ and $\bar{E}_m \sim B_0^2 L_0^2$, so that $E'_m / \bar{E}_m \sim \text{Rm}^{1/3} \approx 8$ here, consistent with Fig. 2. However, for $t \gtrsim 80$, vortex disruption (if it occurs) changes the evolution of the energy. For the undisrupted case ($M = 0.01$), the evolution becomes one of complete flux expulsion (see Fig. 1), with E'_m decreasing to less than \bar{E}_m . (This is different to the well-known theory of [29], in which $E'_m \sim \text{Rm}^{1/2} \bar{E}_m$ in the flux-expelled state, but that kinematic single-vortex theory may not apply to this dynamic regime with a periodic array of vortices and remote boundaries.) For the strongly disrupted case ($M = 0.05$), we enter a different regime, with E'_m staying close to \bar{E}_m throughout the evolution. This regime with persistent small spatial scales results in stronger dissipation: whereas the total dissipation is small and comparable with that of the hydrodynamic case for $M = 0.01$ and 0.03 , it is about three times higher when $M = 0.05$. Further, even though $\bar{E}_m \ll \bar{E}_k$ throughout the evolution for all three cases (i.e., weak large-scale magnetic field), E'_m becomes comparable with E'_k when there is vortex disruption, reflecting the dynamical importance of the small-scale magnetic field.

To calculate the vortex disruption parameter Δ , defined by (23), we first need to evaluate $W(x, y, t)$. This is shown in Fig. 3(a) for the three control runs at $t = 150$, highlighting those regions where either strain or vorticity dominates. Adopting the convention of identifying vortical regions as those where $W < -0.2\sigma$ results in the plots of Fig. 3(b). For $M = 0.01$ and $M = 0.03$, this leads to the identification of a well-defined coherent vortex. For the severely disrupted case of $M = 0.05$ on the other hand, disruption results in a small parent vortex, as well as disconnected vortices and filaments. Our interest is in the disruption to the parent vortex, and so to employ the disruption measure Δ , we need to ignore these resulting by-products. To address this, a further filter is applied, which selects the largest connected region originating from the centre of the parent vortex (which in this case is well defined since the resulting instability has zero phase speed, so the single vortex formed is stationary). The W field is digitised, with all points where $W < -0.2\sigma$ set to one, and all other points set to zero. The MATLAB command `bwlabel` is then applied to the resulting data array to select the connected regions; the connected region originating from the centre of the vortex is then chosen as the region A for the calculation of Δ (see Fig. 3(c)).

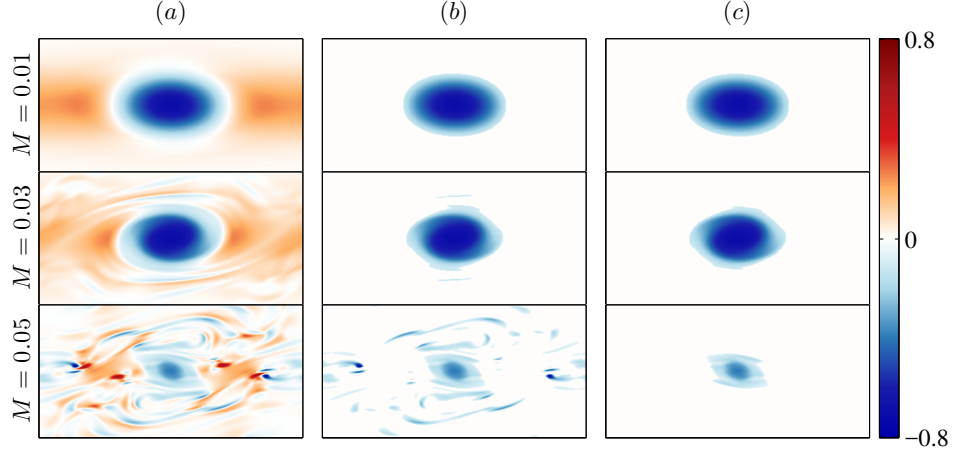


FIG. 3. Okubo–Weiss field for the shear layer corresponding to the $t = 150$ cases shown in Figure 1. (a) The full W field given in equation (22); (b) the field keeping only $W < -0.2\sigma$; (c) a further filtered field keeping only the largest connected region originating from the centre of the parent vortex.

The quantity Δ is computed at $t = 150$ for all simulations detailed in Table I. To test the vortex prediction (12), in Fig. 4 we show Δ versus $M^2\text{Rm}$, from which it can be seen that there is a reassuring collapse of the data. The most important point to note is that for $M^2\text{Rm} \gtrsim 1.5$, the vortices are deemed to have been completely disrupted. This is in agreement with (12), which predicts disruption for $M^2\text{Rm} \sim 1$. Further, for $M^2\text{Rm} \lesssim 1$ we would expect Δ to be monotonically increasing with $M^2\text{Rm}$. Indeed, on performing a regression on the data in the interval $0.1 \leq \Delta \leq 0.9$, we find that $\Delta \sim (M^2\text{Rm})^{1.10}$ (although a different definition of Δ could lead to a different positive exponent).

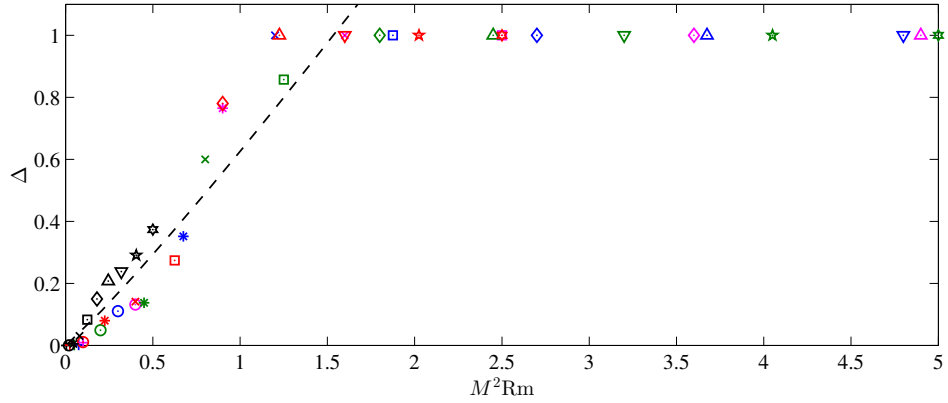


FIG. 4. Δ vs $M^2\text{Rm}$ for the shear layer (colours: varying Rm ; markers: varying M ; see Table I for marker and colour values). The dotted line is obtained from a regression of the data. For display purposes, data beyond $M^2\text{Rm} = 5$ is omitted.

Our focus here has been on the transition from an essentially kinematic regime to a dynamic regime when $M^2 \sim \text{Rm}^{-1} \ll 1$. If M^2 is increased beyond Rm^{-1} , then severe vortex disruption continues for a while, as implied by Fig. 4. However, if M becomes sufficiently large ($M \gtrsim 0.35$ here), then the magnetic field is strong enough to suppress vortex formation completely.

B. Bickley jet

We now consider the disruption of vortices arising from the instability of the Bickley jet, $U(y) = \text{sech}^2(y)$. Linear instabilities of this profile in the hydrodynamic setting are again well documented [39]; there are odd and even modes of instability, with the latter being the most unstable at wavenumber $\alpha_c = 0.90$. In the MHD setting, linear stability is guaranteed for this configuration when $M \geq 0.5$ [50]. This jet profile is known to break up into vortices if the initial field is not so strong that it suppresses

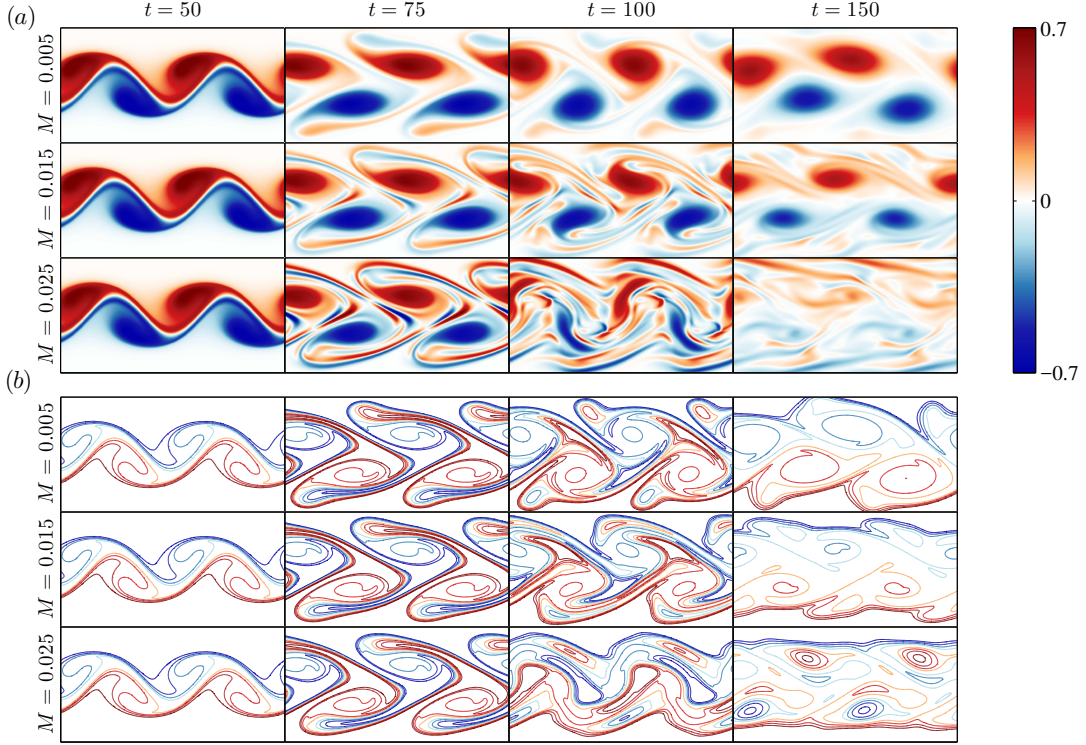


FIG. 5. Snapshots of (a) vorticity and (b) magnetic field lines for the jet at different field strengths (for $Rm = Re = 500$), shown for the central half of the channel ($-L_y/2 \leq y \leq L_y/2$).

the primary hydrodynamic instability; depending on the parameter values, the resulting vortices have been observed to suffer disruption by the magnetic field [11, 13, 15].

The optimum wavenumber $\alpha_c = 0.90$ is roughly twice that of the shear layer case. In order to employ the same resolution as the shear layer case, we consider a channel length that is twice this optimum wavelength. Fifty simulations with parameter values given in Table II were carried out, with the values of M again chosen to lie well below the stabilising value of M ($M \approx 0.3$ for $\alpha = 0.90$, implying lower values of M than for the shear layer). For the Bickley jet, the initial magnetic to kinetic energy ratio is given by $2M^2 L_y / (\int U(y)^2 dy) \approx 15M^2$; this ratio is less than $3/80$ for the values of M considered here.

parameter	values	marker/colour in Fig. 8
M	0.005–0.05, 0.005 spacing	+ ○ * × □ ◇ △ ▽ ☆ ☆, in ascending order
Rm	50, 250, 500, 750, 1000	black, red, green, blue, magenta

TABLE II. Parameter values employed for the jet simulations.

Three control runs are again chosen, with $Rm = 500$ and $M = 0.005, 0.015$ and 0.025 . Fig. 5 shows snapshots of the vorticity and magnetic field lines for the three representative cases. For $M = 0.005$, the evolution is essentially hydrodynamic, with a meandering of the jet before it breaks into two pairs of vortices; MHD feedback is weak and there are no visible disruptions to the vortices. For $M = 0.015$, the vortices at $t = 100$ are slightly distorted by the released magnetic stresses; disruption, however, is not strong enough to destroy the vortices. For $M = 0.025$, the induced magnetic stresses are strong enough to distort the vortices significantly; indeed, the vortex cores have almost disappeared by $t = 150$.

Fig. 6 shows the time series of the energies for the three control runs. The relative sizes of \bar{E}_k , E'_k , \bar{E}_m and E'_m follow the same patterns as for the shear layer. However, in contrast to the shear layer, here the total dissipation is actually lower for the severe vortex disruption case ($M = 0.025$) than for the undisrupted case ($M = 0.005$). As shown in Fig. 5, although the small-scale structures in the vorticity and magnetic field are initially amplified by severe disruption ($t = 100$), which enhances the dissipation, for longer times they are suppressed ($t = 150$).

We calculate Δ using a similar procedure as for the shear layer. However, since four vortices are generated by the instability in this configuration, to calculate the area A for the integral (23) we now select the four largest connected components of $W(x, y)$,

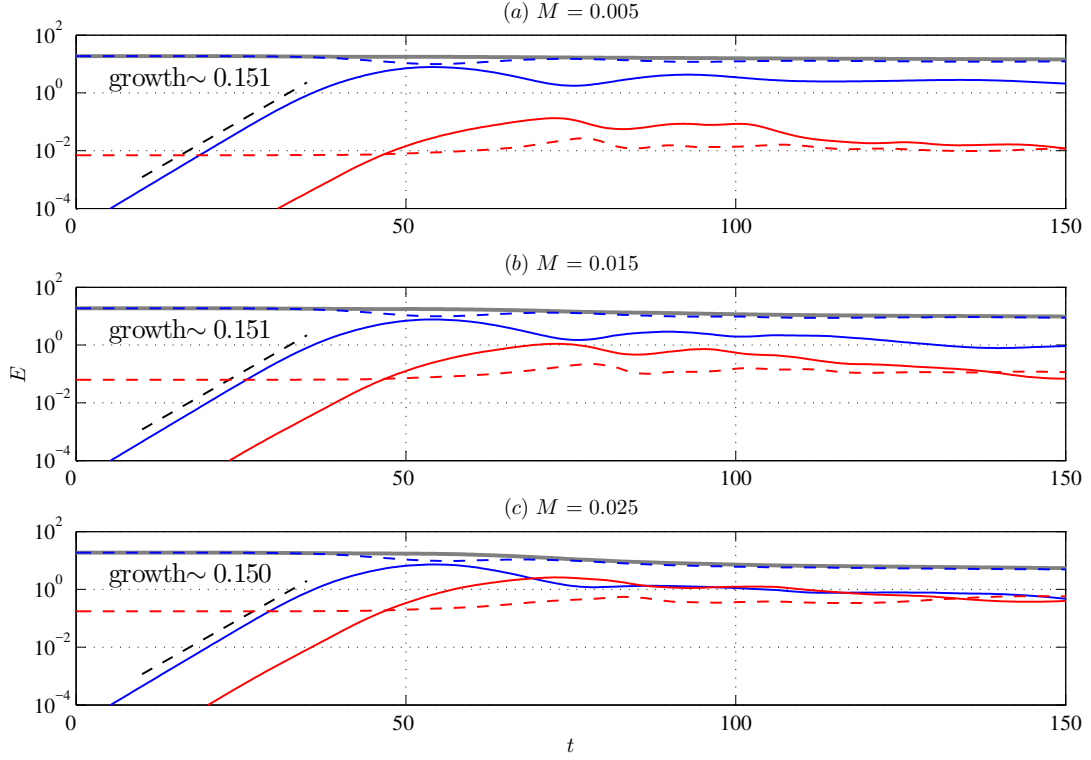


FIG. 6. Time series of the energies (blue = kinetic; red = magnetic; solid = perturbation state; dashed = mean state; grey solid line = total energy) for the jet at different field strengths (for $Rm = Re = 500$).

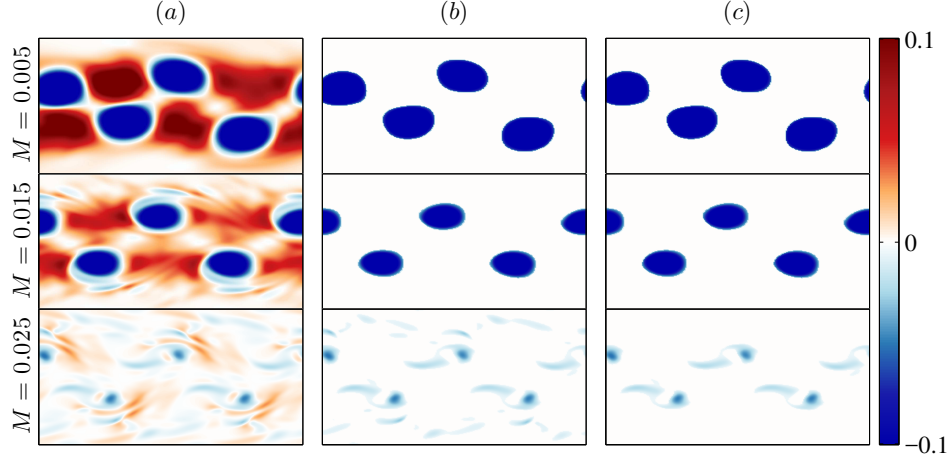


FIG. 7. Okubo–Weiss field for the jet corresponding to the $t = 150$ cases shown in Fig. 5. (a) The full W field given in equation (22); (b) the field keeping only $W < -0.2\sigma$; (c) a further filtered field keeping only the four largest connected components, accounting for periodicity. The colour scale is saturated in order to show the small values when $M = 0.025$.

accounting for periodicity. The procedure is illustrated for the three control runs in Fig. 7, at $t = 150$. When performed for all fifty simulations given in Table II, we obtain the plot of Δ (at $t = 150$) vs M^2Rm given in Fig. 8. It shows the same general characteristics as for the shear layer: there is an approximately linear increase of Δ with M^2Rm ($\Delta \sim (M^2Rm)^{0.94}$) up to a critical value, given by $M^2Rm \approx 0.3$, above which there is complete vortex disruption ($\Delta \approx 1$). Note that for both the shear layer and the jet, the critical value of M^2Rm for complete vortex disruption is of order unity, although the precise value varies from case to case.

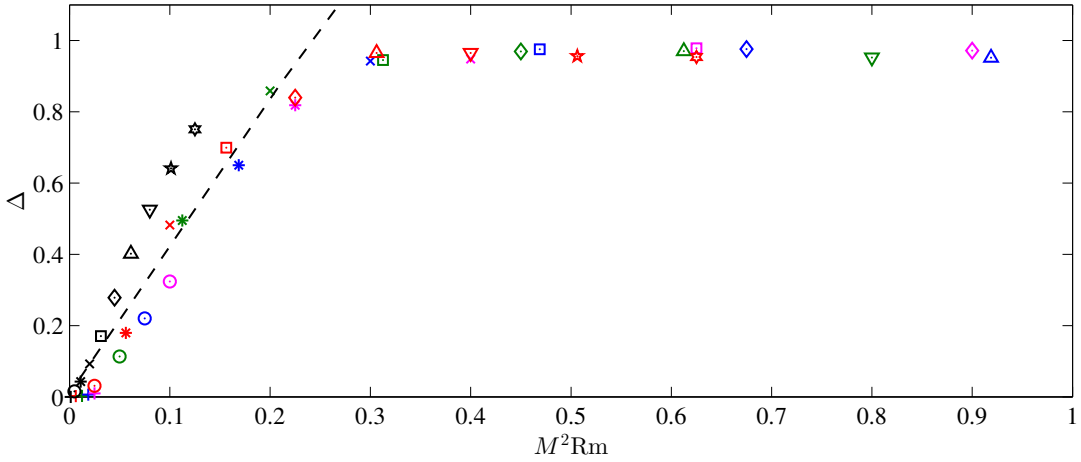


FIG. 8. Δ vs $M^2\text{Rm}$ for the jet (colours: varying Rm ; markers: varying M ; see Table II for marker and colour values). The dotted line is obtained from a regression of the data. For display purposes, data beyond $M^2\text{Rm} = 1$ are omitted.

V. SCALING OF THE LORENTZ FORCE

The derivation of expression (12), the criterion for vortex disruption, requires estimates of the strength and spatial scale of the expelled magnetic field, of the magnitude of the associated Lorentz force and of the competing hydrodynamical forces. In Section II, our argument was presented in terms of force balances in the three-dimensional vorticity and induction equations. The phenomena of flux expulsion and subsequent vortex disruption are, however, primarily two-dimensional — and our numerical simulations are strictly two-dimensional. It is therefore instructive to revisit the scaling arguments in terms of the nondimensional variables ψ and A , as employed in Section III, and in the light of the results of the numerical simulations, described in Section IV.

From the nondimensional vorticity equation (14a) (or, alternatively, (18a)), it is clear that the magnetic field becomes dynamically significant once $M^2 J(A, \nabla^2 A)$ is comparable in magnitude to $J(\psi, \omega)$. Our arguments in Section II focus on what might be considered as the dynamical breakdown of the kinematic regime. At this point, the velocity and vorticity are still large scale, leading to an unambiguous estimate of the magnitude of $J(\psi, \omega)$. By contrast, the expelled magnetic field varies on both large and small scales; determining the size of the $J(A, \nabla^2 A)$ term is thus not so straightforward.

As explained in Section II, flux expulsion leads to magnetic field being confined to a thin strip of width l , along which there are variations in strength on a lengthscale $L_v \gg l$. We therefore need to understand how the Jacobian

$$J(A, \nabla^2 A) = \frac{\partial(A, \nabla^2 A)}{\partial(x, y)} = \frac{\partial A}{\partial x} \frac{\partial}{\partial y} \nabla^2 A - \frac{\partial A}{\partial y} \frac{\partial}{\partial x} \nabla^2 A \quad (24)$$

scales with l and L_v . Unless the field is strictly aligned with one of the x and y axes then each of the two terms on the right hand side of (24) will scale as A^2/l^4 . One might therefore be tempted to assume that

$$J(A, \nabla^2 A) \sim \frac{A^2}{l^4}; \quad (25)$$

however, this significantly overestimates the magnitude of the Jacobian. To see why this is the case, it is instructive to express $J(A, \nabla^2 A)$ in general two-dimensional orthogonal curvilinear coordinates (x_1, x_2) with scale factors (h_1, h_2) , namely

$$J(A, \nabla^2 A) = \frac{1}{h_1 h_2} \left(\frac{\partial A}{\partial x_1} \frac{\partial \nabla^2 A}{\partial x_2} - \frac{\partial A}{\partial x_2} \frac{\partial \nabla^2 A}{\partial x_1} \right), \quad \text{with} \quad \nabla^2 A = \frac{1}{h_1 h_2} \left(\frac{\partial}{\partial x_1} \left(\frac{h_2}{h_1} \frac{\partial A}{\partial x_1} \right) + \frac{\partial}{\partial x_2} \left(\frac{h_1}{h_2} \frac{\partial A}{\partial x_2} \right) \right). \quad (26)$$

Now consider an arbitrary point on the (curved) flux strip, and let (x_1, x_2) be a local orthogonal curvilinear coordinate system in the plane of the strip, with x_1 and x_2 pointing, respectively, across and along the strip. Then, with $h_1^{-1} \partial/\partial x_1 \sim l^{-1}$ and $h_2^{-1} \partial/\partial x_2 \sim L_v^{-1}$, we have $\nabla^2 A \sim A/l^2$, and

$$J(A, \nabla^2 A) \sim \frac{A^2}{l^3 L_v}, \quad (27)$$

a reduction of $O(l/L_v)$ in comparison with the naive estimate (25).

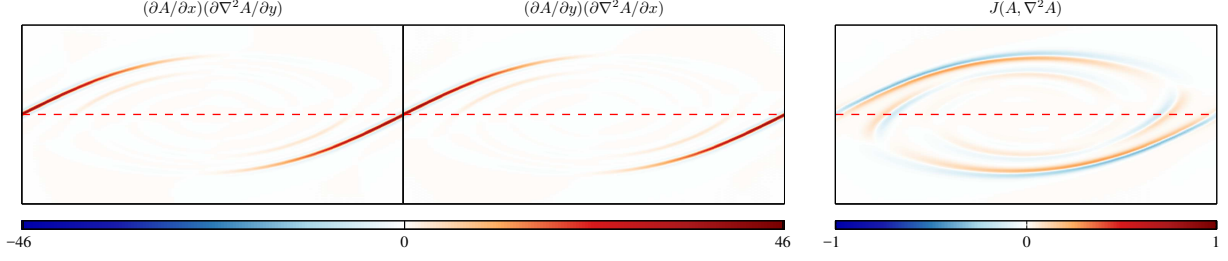


FIG. 9. Decomposition of the components in $J(A, \nabla^2 A)$, for the shear layer simulation $M = 0.05$, $\text{Rm} = 500$, at $t = 55$ (cf. Figure 1a), shown for the central half of the channel ($-L_y/2 \leq y \leq L_y/2$).

In order to test our theoretical predictions quantitatively, we use numerical simulations of the shear layer at a time when strong field has formed at the edge of the vortex, but before disruption occurs. We have chosen $t = 55$ (cf. Fig. 1), although the results are a little sensitive to this choice. Confirmation that, in Cartesian coordinates, significant cancellation between the two component terms of $J(A, \nabla^2 A)$ does indeed take place is provided by Fig. 9, which shows, individually, the magnitudes of the two terms in (24) for one specific case, together with their much smaller difference.

To quantify this reduction across a wide parameter space we evaluate

$$\delta = \frac{\max |J(A, \nabla^2 A)|}{\max |(\partial A/\partial x)(\partial \nabla^2 A/\partial y)|}. \quad (28)$$

If $J(A, \nabla^2 A) \sim A^2/\ell^3 L_v$, as in (27), but the individual components scale as A^2/ℓ^4 , as in (25), we should have a reduction

$$\delta \sim \frac{\ell}{L_v}. \quad (29)$$

For configurations such as shown in Fig. 9 we can independently determine δ , ℓ and L_v . The length scale ℓ is diagnosed by taking a transect at $y = 0$ of $|(\partial A/\partial x)(\partial \nabla^2 A/\partial y)|$ and calculating the half width of the single maximum. The length scale L_v is identified as the mean extent of the vortex as identified by the Okubo–Weiss criterion. Figure 10(a) shows δ as a function of ℓ/L_v for 40 runs with $\text{Rm} \geq 250$. A fitting of the logarithm of this data shows that δ scales as $(\ell/L_v)^{0.930}$, consistent with the prediction in (29). (Note that we have omitted the $\text{Rm} = 50$ points; unsurprisingly, for such a low value of Rm , they do not obey the same relation between δ and ℓ/L_v .)

We are ultimately interested in how $J(A, \nabla^2 A)$ at this time scales with Rm , so we now test the scaling (27) across a wide parameter space. Note that A and L_v are of order unity by the assumed nondimensionalisation, while the nondimensional versions of (2) and (3) are $b\ell \sim 1$ and $b \sim \text{Rm}^{1/3}$, so that $\ell \sim \text{Rm}^{-1/3}$. Our scaling (27) thus implies $J(A, \nabla^2 A) \sim \text{Rm}$ at this time. Figure 10(b) shows the mean value of $\max J(A, \nabla^2 A)$, where the average is taken over all ten values of M at each Rm (see Table I). Omitting the $\text{Rm} = 50$ data, a fitting of the logarithm of this data shows that $\max J(A, \nabla^2 A)$ scales as $\text{Rm}^{1.111}$, consistent with the prediction in (27).

The ordering (27) is essentially equivalent to the ordering (5), although the details of the derivation are slightly different; it thus leads to the estimate (12) for vortex disruption, namely $M^2 \text{Rm} \sim 1$. Were the Lorentz force stronger than estimated by (27), in particular if its strength were given by (25), then a weaker background field would lead to vortex disruption, determined by $M^2 \text{Rm}^{4/3} \sim 1$. Conversely, if the cancellation in expression (24) were extremely strong (i.e. $O(\ell^2/L_v^2)$), leading to an ordering $J(A, \nabla^2 A) \sim A^2/\ell^2 L_v^2$, then the threshold for the dynamic regime would satisfy $M^2 \text{Rm}^{2/3} \sim 1$. It is of interest to note that it is this latter scaling that is identified by Gilbert et al. [28] as the onset of the dynamic regime in their quasi-linear model of flux expulsion.

VI. DYNAMICAL PHENOMENA

We believe that the dynamics underlying the vortex disruption, leading to the estimate (12), is quite general. However, in any given setting, there could be interesting dynamical implications beyond those of the disruption itself. Here, we spell out some of the specific implications for the nonlinear evolution of shear flow instabilities.

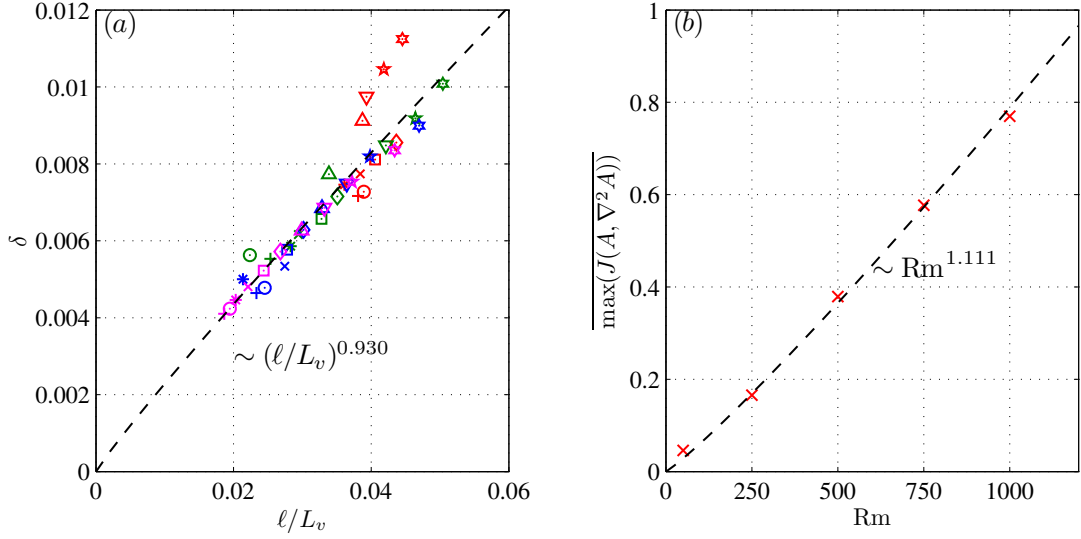


FIG. 10. (a) Plot of δ as defined in (28) against ℓ/L_v , for the $t = 55$ simulation data of the shear layer across all values of M and Rm (colours: varying Rm ; markers: varying M ; see Table I for marker and colour values); the $Rm = 50$ data are not plotted. (b) Plot of the mean value of $\max J(A, \nabla^2 A)$ against Rm , where the average is taken over the ten values of M . Both dotted lines are obtained from a regression of the data with the $Rm = 50$ data omitted.

A. Mean flow changes

A quantity of considerable importance in the instability of shear flows is the mean flow, defined here to be

$$\bar{u}(y, t) = \frac{1}{L_x} \int_0^{L_x} u(x, y, t) dx, \quad (30)$$

where L_x is the channel length. In combination with the magnetic field, the mean flow determines the strength of the initial linear instability, and its evolution with time shows how the nonlinear dynamics act to mix momentum in the cross-stream direction.

Snapshots of \bar{u} for the shear layer and the jet are shown in Fig. 11, for each of the three control runs. For the undisturbed cases (essentially hydrodynamic) in Fig. 11(a, d), the shear is reduced around the centre of the channel as the instability reaches finite amplitude, but the mean flow remains largely unchanged thereafter. For the mildly disrupted cases in Fig. 11(b, e), the behaviour is similar (i.e., essentially hydrodynamic) near the centre of the channel ($|y| \lesssim 2$), but beyond that there is an additional broadening of the mean flow when vortex disruption sets in, for $t \gtrsim 100$. However, for the severely disrupted cases in Fig. 11(c, f), the mean flow evolution is substantially different, with mixing of momentum over a wider region (about twice as wide as for the hydrodynamic case), leaving smaller shears near the centre of the channel. This is consistent with previous studies [e.g., 16].

It is possible to quantify the influence of vortex disruption on the evolving mean flow by measuring the width of the mean flow changes relative to those of the hydrodynamic case [27]. This analysis reveals how the width of the changes to the mean flow increases with $M^2 Rm$, with substantial widening when $M^2 Rm \sim 1$ — i.e., within the vortex disruption regime.

B. Secondary hydrodynamic instabilities

It is well known that vortices generated during the finite-amplitude stage of shear instabilities can be unstable to a range of secondary hydrodynamic instabilities. Our numerical simulations were designed to suppress such secondary hydrodynamic instabilities, so that only magnetic disruption of the vortices could occur. However, within our two-dimensional system, there is the possibility of the subharmonic pairing instability [51–53], which requires two or more vortices in the along-stream direction. For our shear layer simulations, this was completely suppressed, since only a single vortex was generated within the domain. For our jet simulations, where two vortices were generated in the along-stream direction, early signatures of the subharmonic pairing instability may be seen in Fig. 5 for the undisturbed case with $M = 0.005$, and to a lesser extent in the mildly disrupted case with $M = 0.015$. However, in the strongly disrupted case with $M = 0.025$, the magnetic disruption occurs on a faster timescale than the pairing instability, and the disrupted vortices show no signs of pairing. An interesting alternative scenario is

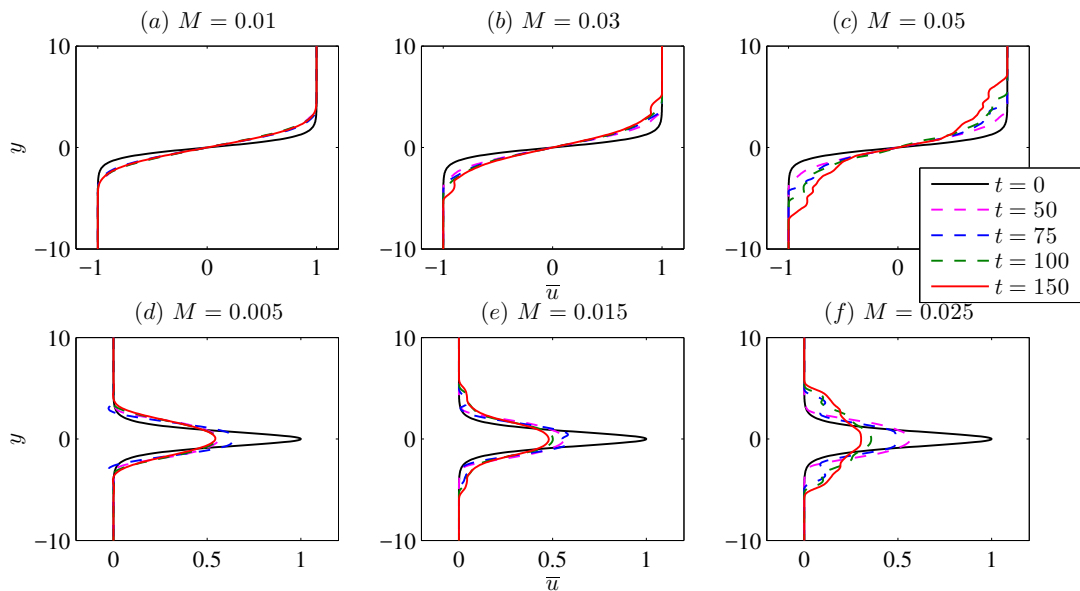


FIG. 11. Snapshots of \bar{u} for the shear layer (a, b, c) and jet (d, e, f) at different field strengths (for $Rm = Re = 500$). Some of the curves lie on top of each other and are indistinguishable.

when magnetic disruption does not act on the primary vortices, but in which repeated subharmonic pairings eventually lead to a large vortex that does suffer magnetic disruption. Although there is evidence of this occurring in studies of longer channels [14], we did not find this in sample simulations where the domain was extended to allow for eight wavelengths of the primary instability.

For different flow configurations, other hydrodynamic secondary instabilities could occur. With a third spatial dimension, there is the possibility of either hyperbolic instabilities on the thin braids between vortices or elliptical instabilities on the vortex cores, as discussed in [54], for example. With density stratification, there is also the possibility of convective type instabilities associated with density overturning in the vortex cores, which compete with various other modes [4, 5]. However, such secondary instabilities are all excluded here through our choice of a two-dimensional system of constant density. In three-dimensional or stratified flows, whether or not such secondary instabilities would act before magnetic disruption of the parent vortices is an open question.

VII. CONCLUSION AND DISCUSSIONS

Of great astrophysical significance is the idea that a very weak large-scale magnetic field, i.e. a field with energy much smaller than the kinetic energy of the flow in question, can still have dynamically significant consequences. Small-scale, typically turbulent, motions distort the large-scale field to generate small-scale magnetic fields, amplifying the field strength by some positive power of the magnetic Reynolds number Rm . Since the defining characteristic of astrophysical plasmas is that $Rm \gg 1$, this implies that weak large-scale magnetic fields cannot simply be ignored. This phenomenon has been explored for the suppression of both turbulent magnetic diffusivity [17, 18, 23, 24] and the turbulent α -effect of mean field electrodynamics [19–22], the inhibition of jet formation in β -plane turbulence [25], and the suppression of large-scale vortices in rapidly rotating convection [26]. Here we have explored how, in another broad class of problems — the disruption of vortices by a weak large-scale field — the same general dynamical processes can occur. By adopting the arguments of [29], we are able to estimate the magnitude of the induced magnetic stresses arising from the stretching of magnetic field lines by the swirling fluid motion, noting that there is a non-trivial cancellation in the curl of the magnetic tension, as supported by numerical and theoretical analyses. Vortices are disrupted when these magnetic stresses released are sufficiently large; this occurs when $M^2 Rm \sim 1$, where M^2 measures the energy of the large-scale field relative to the kinetic energy. Thus when $Rm \gg 1$, vortex disruption occurs for $M \ll 1$.

The estimate for vortex disruption, $M^2 Rm \sim 1$, is widely applicable for vortex dynamics, however the vortices may arise. Here we test the criterion in detail by considering one of the most important means of vortex generation — the nonlinear development of shear instabilities. We focus on two-dimensional, homogeneous, incompressible MHD, considering in detail two prototypical shear flows (the hyperbolic tangent shear layer and the Bickley jet) with a weak background magnetic field.

The instability of both these flows leads to a periodic array of vortices, which can be prone to magnetic disruption. We first identify coherent vortices by the Okubo–Weiss procedure, which provides a simple definition of vortices as those regions where vorticity dominates over strain, and then construct a measure of disruption Δ by comparison with the purely hydrodynamic evolution. By performing fifty simulations to cover a range of M ($0.01 \leq M \leq 0.1$ for the shear layer and $0.005 \leq M \leq 0.05$ for the jet) and Rm ($50 \leq Rm \leq 1000$) at $Re = 500$, we are able to investigate the dependence of Δ on both M and Rm . For both shear flows, we find an approximate linear increase of Δ with $M^2 Rm$ up to a critical value of $M^2 Rm$ of order unity, followed by a sharp transition to a regime in which $\Delta \approx 1$, denoting total disruption of the vortices. These numerical results are in excellent agreement with the theoretical estimate. Our theoretical ideas are also supported by inspection of the energy time series, which show that disruption is characterised by an ordering in which the energies of the perturbed magnetic field, the mean field, and the perturbed flow are comparable (but all much less than the kinetic energy of the unperturbed shear flows).

The disruption estimate $M^2 Rm \sim 1$, first derived in [27], is in contrast to the result more recently reported in [28]. In that work, which considers the dynamical feedback of a vortex in a magnetic field, in a quasi-linear setting assuming azimuthal symmetry, the breakdown of the kinematic argument, and thus the regime where vortex disruption may be expected to take place, occurs when $M^2 Rm^{2/3} \sim 1$ in our notation. Since our set of simulation data takes Rm values between 50 and 1000, distinguishing between the asymptotic scalings $M^2 Rm$ and $M^2 Rm^{2/3}$ is difficult. That said, it is interesting to note, following our line of argument in Section V, that if the curl of the magnetic tension were to scale as b^2/L_v^2 , rather than $b^2/\ell L_v$ as we suggest, then the resulting disruption estimate would indeed be $M^2 Rm^{2/3} \sim 1$. Given that both our theoretical and numerical analyses support the scaling of the curl of the magnetic tension as $b^2/\ell L_v$, the difference in the asymptotic scaling for disruption is perhaps attributable to differences between a fully nonlinear system and a quasi-linear system with imposed symmetry.

Further, the vortex disruption estimate depends crucially on a balance between advection and dissipation of small-scale field. Since dissipation is represented by a Laplacian operator in the induction equation, estimate (12) involves an explicit dependence on Rm . This dependence is captured by our numerical approach, which uses a Laplacian diffusion operator with resolution down to the dissipation scale. Numerical schemes with alternative (non-Laplacian) prescriptions for the dissipation would presumably realise vortex disruption in a somewhat different way.

The notion of vortex disruption has some interesting astrophysical implications. Since the derived estimate for disruption is $M^2 Rm \sim 1$, and Rm is typically extremely large in astrophysical systems, vortex disruption should be a robust dynamical feature. If vortex disruption does occur, it is likely to lead to mixing of quantities such as angular momentum, heat and passive scalars, with implications for the large-scale angular velocity, temperature and chemical composition. Of particular note is that in systems such as the solar tachocline, constrained by stable stratification, many of the standard mixing scenarios do not occur. However, provided there are vortices, we have shown that their interaction with a magnetic field can provide an alternative route to mixing. The theoretical disruption estimate (12) assumes that $Rm \gg 1$ and implicitly assumes that the flow is smooth on the small scales of the field; this equates to an assumption that the magnetic Prandtl number $Pm = \nu/\eta = Rm/Re \gtrsim O(1)$. Whereas this does indeed hold in the interstellar medium, in stellar interiors $Pm \ll 1$. Although one could envisage vortex disruption by a similar physical mechanism in this regime, the line of argument leading to a disruption estimate would need to be modified. Furthermore, the testing of any such hypothesis in the regime $Re \gg Rm \gg 1$ is currently computationally unattainable.

ACKNOWLEDGMENTS

JM was supported by the STFC Doctoral Training Grant ST/F006934/1, the ISF grant 1537/12 and the NERC grant NE/L005166/1. We thank Andrew Gilbert for helpful comments, which led to further analysis and a subsequent improvement of this article.

-
- [1] B. Favier, L. J. Silvers, and M. R. E. Proctor, “Inverse cascade and symmetry breaking in rapidly rotating Boussinesq convection,” *Phys. Fluids* **26**, 096605 (2014).
 - [2] C. Guervilly, D. W. Hughes, and C. A. Jones, “Large-scale vortices in rapidly rotating Rayleigh–Bénard convection,” *J. Fluid Mech.* **758**, 407–435 (2014).
 - [3] A. Mashayek and W. R. Peltier, “Three-dimensionalization of the stratified mixing layer at high Reynolds number,” *Phys. Fluids* **23**, 111701 (2011).
 - [4] A. Mashayek and W. R. Peltier, “The ‘zoo’ of secondary instabilities precursory to stratified shear flow transition. Part 1 Shear aligned convection, pairing, and braid instabilities,” *J. Fluid Mech.* **708**, 5–44 (2012).
 - [5] A. Mashayek and W. R. Peltier, “The ‘zoo’ of secondary instabilities precursory to stratified shear flow transition. Part 2 The influence of stratification,” *J. Fluid Mech.* **708**, 45–70 (2012).
 - [6] J. Mak, S. D. Griffiths, and D. W. Hughes, “Shear flow instabilities in shallow-water magnetohydrodynamics,” *J. Fluid Mech.* **788**, 767–796 (2015).
 - [7] C.-M. Ho and P. Huerre, “Perturbed free shear layers,” *Annu. Rev. Fluid Mech.* **16**, 365–424 (1984).

- [8] A. Malagoli, G. Bodo, and R. Rosner, “On the nonlinear evolution of magnetohydrodynamic Kelvin–Helmholtz instabilities,” *Astrophys. J.* **456**, 708–716 (1996).
- [9] A. Frank, T. W. Jones, D. Ryu, and J. B. Gaalaas, “The MHD Kelvin–Helmholtz instability: A two-dimensional numerical study,” *Astrophys. J.* **460**, 777–793 (1996).
- [10] T. W. Jones, J. B. Gaalaas, D. Ryu, and A. Frank, “The MHD Kelvin–Helmholtz instability. II. The role of weak and oblique fields in planar flows,” *Astrophys. J.* **482**, 230–244 (1997).
- [11] D. Biskamp, E. Schwarz, and A. Zeiler, “Instability of a magnetized plasma jet,” *Phys. Plasmas* **5**, 2485–2488 (1998).
- [12] R. Keppens, G. Toth, R. H. J. Westermann, and J. P. Goedbloed, “Growth and saturation of the Kelvin–Helmholtz instability with parallel and anti-parallel magnetic fields,” *J. Plasma Phys.* **61**, 1–19 (1999).
- [13] H. Baty and R. Keppens, “Interplay between Kelvin–Helmholtz and current-driven instabilities in jets,” *Astrophys. J.* **580**, 800–814 (2002).
- [14] H. Baty, R. Keppens, and P. Comte, “The two-dimensional magnetohydrodynamic Kelvin–Helmholtz instability: Compressibility and large-scale coalescence effects,” *Phys. of Plasmas* **10**, 4661–4674 (2003).
- [15] H. Baty and R. Keppens, “Kelvin–Helmholtz disruptions in extended magnetized jet flows,” *Astron. Astrophys.* **447**, 9–22 (2006).
- [16] M. L. Palotti, F. Heitsch, E. G. Zweibel, and Y. M. Huang, “Evolution of unmagnetized and magnetized shear layers,” *Astrophys. J.* **678**, 234–244 (2008).
- [17] S. I. Vainshtein and R. Rosner, “On turbulent diffusion of magnetic fields and the loss of magnetic flux from stars,” *Astrophys. J.* **376**, 199–203 (1991).
- [18] F. Cattaneo and S. I. Vainshtein, “Suppression of turbulent transport by a weak magnetic field,” *Astrophys. J.* **376**, L21–L24 (1991).
- [19] R. M. Kulsrud and S. W. Anderson, “The spectrum of random magnetic fields in the mean field dynamo theory of the Galactic magnetic field,” *Astrophys. J.* **396**, 606–630 (1992).
- [20] L. Tao, F. Cattaneo, and S. I. Vainshtein, “Evidence for the suppression of the α -effect by weak magnetic fields,” in *Solar and Planetary Dynamos*, edited by M. R. E. Proctor, P. C. Matthews, and A. M. Rucklidge (Cambridge University Press, 1993) pp. 303–310.
- [21] A. V. Gruzinov and P. H. Diamond, “Self-consistent theory of mean-field electrodynamics,” *Phys. Rev. Lett.* **72**, 1651–1653 (1994).
- [22] F. Cattaneo and D. W. Hughes, “Nonlinear saturation of the turbulent α effect,” *Phys. Rev. E* **54**, 4532–4535 (1996).
- [23] S. R. Keating, L. J. Silvers, and P. H. Diamond, “On cross-phase and the quenching of the turbulent diffusion of magnetic fields in two dimensions,” *Astrophys. J.* **678**, L137–L140 (2008).
- [24] T. Kondić, D. W. Hughes, and S. M. Tobias, “The decay of a weak large-scale magnetic field in two-dimensional turbulence,” *Astrophys. J.* **823**, 111 (2016).
- [25] S. M. Tobias, P. H. Diamond, and D. W. Hughes, “ β -plane magnetohydrodynamic turbulence in the solar tachocline,” *Astrophys. J.* **667**, L113–L116 (2007).
- [26] C. Guervilly, D. W. Hughes, and C. A. Jones, “Generation of magnetic fields by large-scale vortices in rotating convection,” *Phys. Rev. E* **91**, 041001 (2015).
- [27] J. Mak, *Shear Instabilities in Shallow-Water Magnetohydrodynamics*, Ph.D. thesis, University of Leeds (2013).
- [28] A. D. Gilbert, J. Mason, and S. M. Tobias, “Flux expulsion with dynamics,” *J. Fluid Mech.* , 568–588 (2016).
- [29] N. O. Weiss, “The expulsion of magnetic flux by eddies,” *Proc. Roy. Soc. Lond. A* **293**, 310–328 (1966).
- [30] R. R. Kerswell, “Elliptical instability,” *Annu. Rev. Fluid Mech.* **34**, 83–113 (2002).
- [31] M. Rieutord, “Evolution of rotation in binaries: physical processes,” in *Stellar Rotation*, Vol. 215, edited by A. Maeder and P. Eenens (Proc. IAU Symp., 2004) pp. 394–403.
- [32] N. R. Lebovitz and E. Zweibel, “Magnetoelliptic instabilities,” *Astrophys. J.* **609**, 301–312 (2004).
- [33] K. A. Mizerski and K. Bajer, “The magnetoelliptic instability of rotating systems,” *J. Fluid Mech.* **632**, 401–430 (2009).
- [34] A. Okubo, “Horizontal dispersion of floatable particles in the vicinity of velocity singularity such as convergences,” *Deep-Sea Res.* **17**, 445–454 (1970).
- [35] J. Weiss, “The dynamics of enstrophy transfer in two dimensional hydrodynamics,” *Physica D* **48**, 273–294 (1991).
- [36] H. K. Moffatt and H. Kamkar, “On the time-scale associated with flux expulsion,” in *Stellar and Planetary Magnetism*, edited by A. M. Soward (Gordon and Breach, 1983).
- [37] D. J. Galloway, M. R. E. Proctor, and N. O. Weiss, “Magnetic flux ropes and convection,” *J. Fluid Mech.* **87**, 243–261 (1978).
- [38] D. J. Galloway and D. R. Moore, “Axisymmetric convection in the presence of a magnetic field,” *Geophys. Astrophys. Fluid Dyn.* **12**, 73–105 (1979).
- [39] P. G. Drazin and W. H. Reid, *Hydrodynamic Stability*, 2nd ed. (Cambridge University Press, 1981).
- [40] O. Thual, *Transition vers la Turbulence dans des Systèmes Dynamique Apparents à la Convection*, Ph.D. thesis, Université de Nice-Sophia Antipolis (1986).
- [41] S. A. Orszag, “On the elimination of aliasing in finite-difference schemes by filtering high-wavenumber components,” *J. Atmos. Sci.* **28**, 1074 (1971).
- [42] C. Canuto, M. Y. Hussaini, A. Quarteroni, and T. A. Zang, *Spectral Methods in Fluid Dynamics* (Springer, 1993).
- [43] R. Peyret, *Spectral Methods for Incompressible Viscous Flow* (Springer AMS, 2002).
- [44] G. Haller, “An objective definition of a vortex,” *J. Fluid Mech.* **525**, 1–26 (2005).
- [45] D. B. Chelton, M. G. Schlax, and R. M. Samelson, “Global observations of nonlinear mesoscale eddies,” *Prog. Oceanog.* **91**, 167–216 (2011).
- [46] G. Haller, A. Hadjighasem, M. Farazmand, and F. Huhn, “Defining coherent vortices objectively from the vorticity,” *J. Fluid Mech.* **795**, 136–173 (2016).
- [47] J. Isern-Fotanet, E. Garcia-Ladona, and J. Font, “Vortices of the Mediterranean Sea: an altimetric perspective,” *J. Phys. Oceanogr.* **36**, 87–103 (2006).
- [48] D. W. Waugh, E. R. Abraham, and M. M. Bowen, “Spatial variations of stirring in the surface ocean: a case study of the Tasman Sea,” *J.*

Phys. Oceanogr. **36**, 526–542 (2006).

- [49] V. A. Vladimirov, H. K. Moffatt, and K. I. Ilin, “On general transformations and variational principles for the magnetohydrodynamics of ideal fluids. Part 2. Stability criteria for two-dimensional flows,” J. Fluid Mech. **329**, 187–205 (1996).
- [50] D. W. Hughes and S. M. Tobias, “On the instability of magnetohydrodynamic shear flows,” Proc. R. Soc. Lond. A **457**, 1365–1384 (2001).
- [51] R. E. Kelly, “On the stability of an inviscid shear layer which is periodic in space and time,” J. Fluid Mech. **27**, 657–689 (1967).
- [52] J. Jimenez, “On the linear stability of the inviscid Kármán vortex street,” J. Fluid Mech. **178**, 177–194 (1987).
- [53] J. Jimenez, “Linear stability of a non-asymmetric, inviscid, Kármán street of small uniform vortices,” J. Fluid Mech. **189**, 337–348 (1988).
- [54] C. P. Caulfield and W. R. Peltier, “The anatomy of the mixing transition in homogeneous and stratified free shear layers,” J. Fluid Mech. **413**, 1–47 (2000).